Front. Earth Sci. 2025, 19(1): 5−12
https://doi.org/10.1007/s11707-022-0984-3

RESEARCH ARTICLE

# Chlorophyll bloom enhanced by a mesoscale eddy in the western South China Sea

**Yongqiang CHEN[1,2,3], Dajun QIU[1,2,3], Peter CORNILLON[4], Meilin WU (✉)[1,2,3]**

1 State Key Laboratory of Tropical Oceanography and Key Laboratory of Marine Bio-resources Sustainable Utilizing, South China Sea Institute of Oceanology, Chinese Academy of Sciences, Guangzhou 510301, China
2 Southern Marine Science and Engineering Guangdong Laboratory (Guangzhou), Guangzhou 511458, China
3 Innovation Academy of South China Sea Ecology and Environmental Engineering, Chinese Academy of Sciences, Guangzhou 510301, China
4 Graduate School of Oceanography, the University of Rhode Island, Narragansett, RI 02882, USA



**Abstract** Remote sensing of ocean color is used to detect phytoplankton blooms and oceanic eddies. In this study, satellite remote sensing was used to detect an eddy-like phytoplankton bloom in the western South China Sea in early September, 2007. The eddy-like phytoplankton bloom formed in the middle of August, before the formation of a cyclonic eddy. The time series reveals a lag period of about 1 week between maximum chlorophyll (Chl *a*) and maximum eddy intensity. This lag may have been related to the Mekong River discharge and its subsequent mixing by the cyclonic eddy. The spatial distribution of the bloom was characterized by a jet of high Chl *a*. Our data provide evidence that a significant proportion of south-westerly monsoon driven nutrients are used by phytoplankton. We also determined that phytoplankton blooms may support the large-scale advective spreading of high biomass waters to the open ocean by large surface currents. These biomass rich waters are probably important in the food chain dynamics of the outer south-eastern shelf and the coral islands or atolls in the open ocean.

**Keywords** cyclonic eddy, chlorophyll *a*, western South China Sea, remote sensing, phytoplankton

## 1 Introduction

Mesoscale eddies are common and extremely energetic occurrences in the world's seas (McGillicuddy, 2016) that can have significant biogeochemical consequences (Klein and Lapeyre, 2009). Mesoscale eddies have been associated with spatially and temporally transient pulses of nutrient input, enhanced primary productivity, changes in phytoplankton community structure, and the vertical export of organic matter (McGillicuddy et al., 1999; Siegel et al., 1999). In comparison to surrounding seas, cyclonic eddies have domed isopycnals, lower sea surface height, and colder sea surface temperature (SST), whereas anticyclonic eddies have depressed isopycnals, higher sea surface height, and warmer SST (Chen et al., 2021). Eddies are divided into two types: warm eddies and cold eddies. Cold eddies are thought to stimulate phytoplankton growth and export carbon from the euphotic zone more efficiently than warm eddies (Bibby and Moore, 2011; Mourino-Carballido, 2009).

The mixing of surface and deep water provides enough nutrients to produce a high chlorophyll (Chl *a*) level at the subsurface layer's base (Kim et al., 2012). In a cold eddy, nutrient-rich deep water is carried upstream by upbowed isopycnals along the borders of anticyclonic eddies, which produces high Chl *a* concentrations (Mizobata et al., 2002). During the spring months between 1998 and 2002 in the Gulf of Alaska, approximately 80% of the chlorophyll was associated with mesoscale eddies that occupied just 10% of the area of pelagic waters (Crawford et al., 2007). Eddies and filaments carried 40%–50% of the total amount of nutrients provided (Shenoi et al., 2004). Compared to the Tasman Sea, the average Chl *a* for cyclonic eddies was 28% lower, while the average Chl *a* for anticyclonic eddies was 16% greater in Eddy Avenue (Everett et al., 2012).

The South China Sea (SCS) is the largest semi-enclosed sea in the western tropical Pacific Ocean. It has a total area of 3.5 million km$^2$ (Xie et al., 2003; Wang et al., 2009). In summer, the SCS, which is generally stratified, tropical, and oligotrophic, has low phytoplankton biomass (Tang et al., 2004a, 2004b; Chen and Tang, 2012). In the ocean, physical and biogeochemical processes are closely

Received November 14, 2021; accepted February 21, 2022

E-mail: mlwu@scsio.ac.cn

linked. Biochemical fluxes are associated with physical characteristics such as the wind, currents, mixed layer depth, and temperature (Tang et al., 2002; Qiu et al., 2019). Eddies transport heat, salt, and other chemical substances and change dynamic conditions in the ocean (Chen et al., 2010). Mesoscale eddies play an important role in the biogeochemical cycle of the ocean, especially in oligotrophic tropical zones (Chen et al., 2010; Hu et al., 2011; Wang et al., 2016,Sun et al., 2022,Wu et al., 2022a, 2022b). The vertical pumping of nutrients associated with a cold eddy can fuel an eddy-like phytoplankton bloom. However, there have been few observations of phytoplankton blooms with an eddy-like shape that exhibit the dynamics of a cold eddy (Chen and Tang, 2012), especially in the SCS. After using satellite remote-sensing data to search for and analyze many cases of mesoscale eddies in the SCS, we have identified a case of a phytoplankton bloom with an eddy-like shape coinciding with a cold cyclonic eddy in the western SCS. In this paper, we address how the phytoplankton bloom transformed into an eddy-like bloom and what role the cold cyclonic eddy played in the transport of the river plume of phytoplankton to the open ocean. This study will help to improve our understanding of the mechanism behind phytoplankton response to cold cyclonic eddies and the transport of the Mekong River plume in response to cold cyclonic eddies.

## 2 Data

### 2.1 Sea surface Chl *a* concentration

Standard Level 2 products of the Moderate Resolution Imaging Spectroradiometer (MODIS) (1 km × 1 km) were obtained from the National Aeronautics and Space Administration's Ocean Color Working Group's website and were processed using the SeaWiFS Data Analysis System (SeaDAS) (Baith et al., 2001). The bloom patch appeared between 110°E and 112°E and 11.5°N–13.5°N, where the depth of the water was approximately 2000 m (Fig. 1).

### 2.2 Sea surface temperature

Sea surface temperature data were derived from the output of the Asia and Indian–Pacific Ocean (AIPOcean1.0) model. The AIPOcean1.0 is based on the Hybrid Coordinate Ocean Model (HYCOM), which evolved from the Miami Isopycnic Coordinate Ocean Model (MICOM).

### 2.3 Sea surface wind

Data on wind speed and direction over the ocean surface were retrieved from QuikScat measurements of back-scattered power (Wentz et al., 2001). Daily wind speed data were provided by Remote Sensing Systems (RSSs, available at REMSS website).

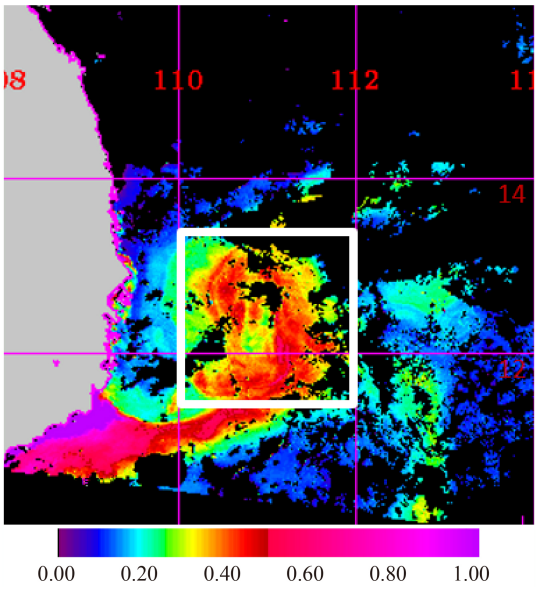


**Fig. 1** MODIS derived sea surface Chl *a* concentration on 28 August 2007. White box shows the sampling area for time series analyzed data.

### 2.4 Sea surface currents

Data on near-real-time sea surface currents (SSCs) and sea height anomalies (SHAs) were provided by the National Oceanic and Atmospheric Administration/ National Ocean Service (NOAA/NOS; available at NOAA website). This field is derived from a three-year global ocean model, the Ocean Circulation and Climate Advanced Modeling project (OCCAM) run driven with realistic European Centre for Medium-Range Weather Forecasts (ECMWF) winds.

### 2.5 Precipitation

Precipitation was estimated using TMPA-RT 3B42RT data with 0.25° × 0.25° spatial resolution. Daily precipitation regimes were provided by the Tropical Rainfall Measuring Mission (TRMM) Online Visualization and Analysis System (TOVAS), developed by Goddard Earth Sciences (GES) and the Distributed Active Archive Center (DAAC) (available at NASA website).

## 3 Results

### 3.1 Eddy-like phytoplankton bloom dynamics

Normally, Chl *a* levels in the western SCS are less than 0.15 mg·m$^{-3}$ (Fig. 2(a)). In the open ocean, a phytoplankton bloom is defined as Chl *a* concentration greater than 0.4 mg·m$^{-3}$. MODIS data revealed a large-scale cyclonic eddy-like augmentation of Chl *a* (Figs. 2(b)–2(h)) on August 7, 2007 (Fig. 2(a)). The bloom was initially noticed on August 21 (Fig. 2(b)) when cloud-free

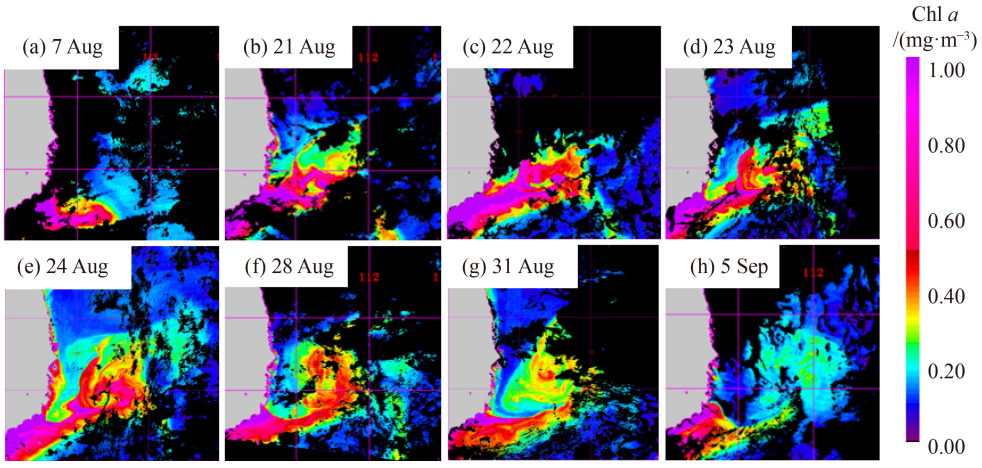


**Fig. 2** MODIS derived sea surface Chl *a* concentration. (a) Before the formation of the cyclonic eddy-like phytoplankton bloom; (b)–(e) form and mature of the eddy-like bloom; (f)–(h) decay of the bloom (black areas: no data).

photos revealed that the Chl *a* concentration had reached 1.4 mg·m$^{-3}$. On August 24 and 28, the bloom displayed a regular, elliptic, cyclonic eddy-like pattern (Figs. 2(e) and 2(f)). The Chl *a* biomass at the eddy's core shows as a low-value circle surrounded by higher value circles on its periphery (Figs. 2(d)–2(f)). On August 28, the high Chl *a* center was located at 12.5°N, 111°E (Fig. 2(f)). The region of Chl *a* > 0.2 mg·m$^{-3}$ was about 48400 km$^2$, with a diameter of roughly 220 km. On August 22, the greatest Chl *a* value in the bloom was 6.7 mg·m$^{-3}$ (Fig. 2(c)). The plume drifted easterly, extending to 111.5°E, and then flowed to the western SCS with a large cyclonic circulation pattern. Ultimately, it decayed due to nutrient exhaustion and gradually disappeared when the south-eastern monsoon weakened (Figs. 2(f)–2(h)).

### 3.2 Cold cyclonic eddy

After a transitory formation stage between August 22 and 29 (Figs. 5(c)–5(f)), the cyclonic eddy became apparent in the dynamic height field on 26 August, intensified over 10 days to reach its maximum with a steady center (110.8°E, 12.2°N, Fig. 5(f)), and then decayed rapidly and dissipated from September 12 to 19. The horizontal scale of the eddy was between 60 and 90 km. The eddy moved slightly eastward after its formation on August 26–28 and then became stable centered near 110.8°E, 12.2°N. More details concerning the eddy's physical dynamic mechanisms can be found in Hu et al. (2011) and Wang et al. (2016). Details about the Mekong River plume can be found in Chen et al. (2010).

### 3.3 Sea surface temperature

Prior to the formation of the eddy, SST was slightly higher at the location of the eddy center than in the surrounding water (Fig. 3(a)). This temperature surface signature was not evident after the eddy formed (Figs. 3(b)–3(g)). Hu et al. (2011) suggested that due to surface heating and the Mekong River (MR) plume, the surface signature of this eddy was not as obvious as the signature below 25 m. Our results support this hypothesis. After September 2, a low SST cold core appeared at the surface (Fig. 3(h)), probably due to wind-induced vertical mixing (discussed in Section 3.6).

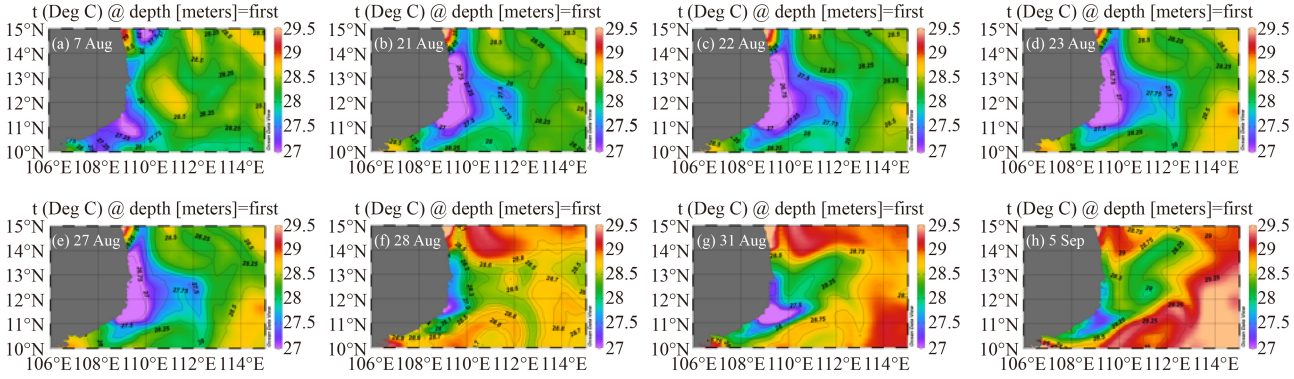


**Fig. 3** Reanalyzed sea surface temperature. (a) Before the formation of the cyclonic eddy-like phytoplankton bloom; (b)–(e) form and mature of the eddy-like bloom; (f)–(h) decay of the bloom.

### 3.4 Sea surface salinity

Prior to the formation of the cyclonic eddy, sea surface salinity (SSS) was slightly higher in the eddy center location than in the surrounding water (Fig. 4(a)). In the surface layer, the MR plume intruded along the jet, and tongue-like low salinity water appeared in the south-western corner of the cyclonic eddy (Figs. 4(b)–4(e)). The salinity field at the edge of the eddy was likely modified by horizontal entrainment of the north-eastward river plume, which moved the surface high salinity center closer to the coast (Figs. 4(f) and 4(g)). The low salinity tongue persisted during the existence of the eddy (Figs. 4(f)–4(h)).

### 3.5 Sea surface height and currents

SSH and currents derived from the OCCAM show that sea surface currents in the bloom area did not have an eddy-like shape prior to eddy formation (Figs. 5(a)–5(f)). Currents in the blooming area did have a cyclonic shape after August 31 (Figs. 5(g)–5(h)), suggesting a cyclonic cold eddy. On August 28, the eddy-like phytoplankton bloom corresponded well with the surface currents in shape, especially in the high-speed area (Fig. 2(f)). Mean sea surface height reached a low value of 0.098 m on August 29, which indicted the formation of the cold cyclonic eddy, 8 days after the mean Chl *a* concentration maximum appeared on August 21 (Fig. 7).

### 3.6 Sea surface wind

Daily QuikScat wind speed data were obtained from August 15 to September 12 (Fig. 6). Low speed south-westerly winds were detected from August 23 to 27, 2007. This low wind speed corresponds to a decrease of the Chl *a* concentration in the eddy area (Fig. 2). The Chl *a* bloom same as the decrease of the sea surface wind speed (e.g., the width of the Chl *a* bloom showed noticeably narrower than that of the jet before 23 August) during the weaken wind (Figs. 2(c)–2(f)). The wind speed increased from August 28 to September 4. Low speed winds were observed from September 5 to 8 (Figs. 2(f)–2(h)), after which the wind speed strengthened again. Mean wind speed in the south-west part of the bloom area reached a maximum of 9.97 $m \cdot s^{-1}$ on August 15 and remained at that level for about 10 days. Six days after this high wind

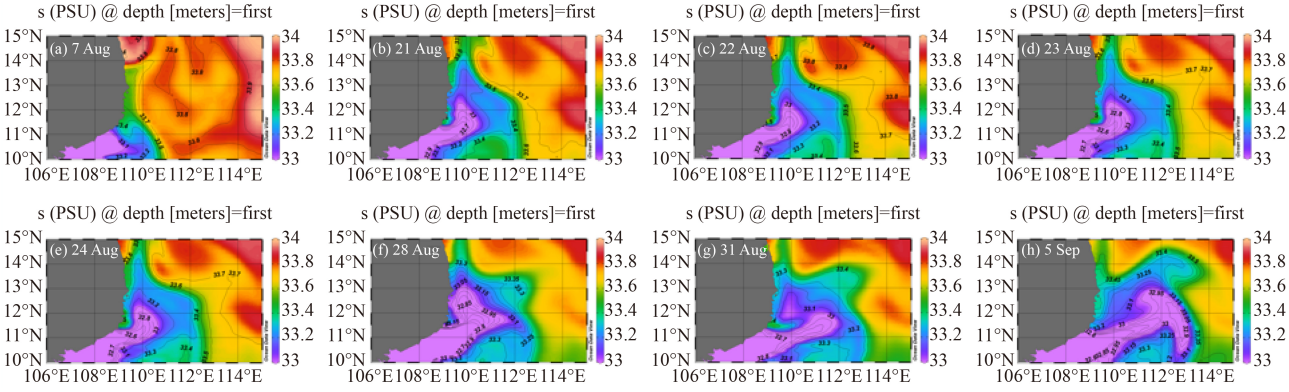


**Fig. 4** Reanalyzed sea surface salinity. (a) Before the formation of the cyclonic eddy-like phytoplankton bloom; (b)–(e) form and mature of the eddy-like bloom; (f)–(h) decay of the bloom.

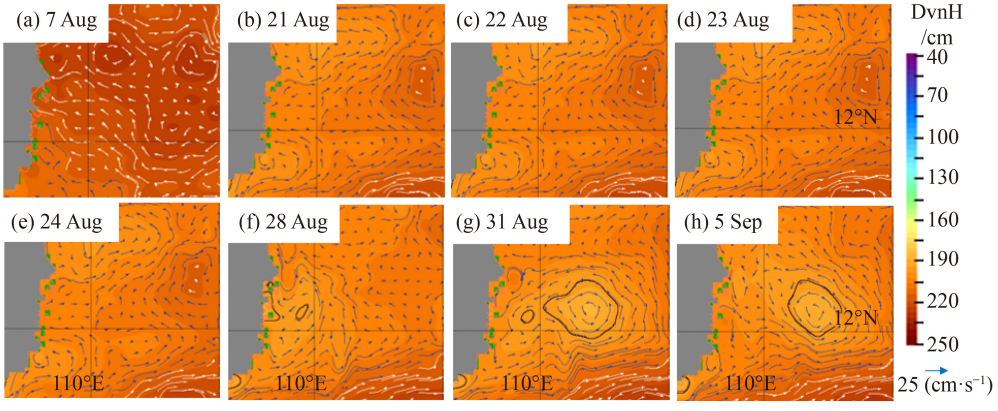


**Fig. 5** Sea-surface currents. (a) Before the formation of the cyclonic eddy-like phytoplankton bloom; (b)–(e) form and mature of the eddy-like bloom; (f)–(h) decay of the bloom.

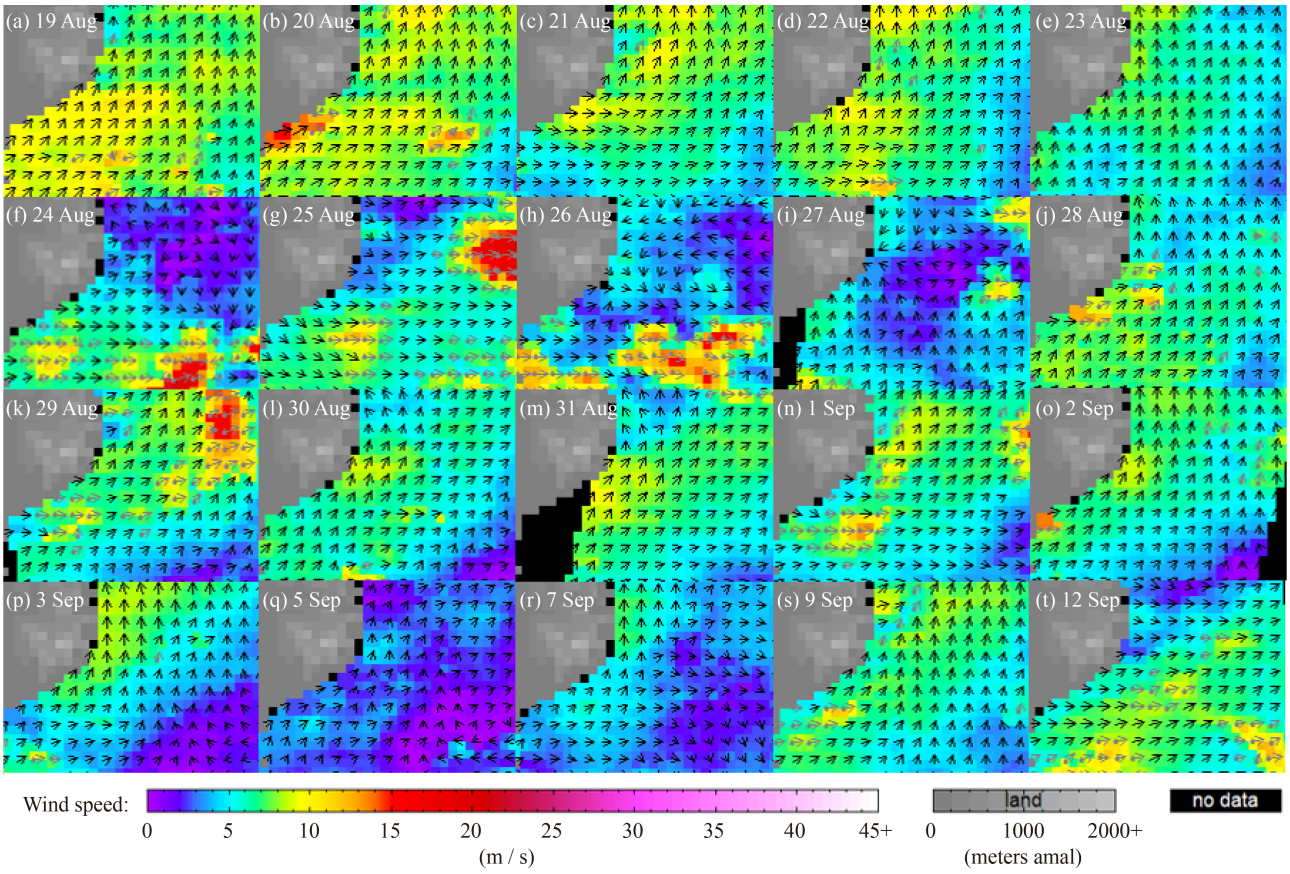


**Fig. 6** Sea-surface winds. (a)–(b) Before the formation of the cyclonic eddy-like phytoplankton bloom; (c)–(e) form and mature of the eddy-like bloom; (f)–(t) decay of the bloom.

speed (on August 21), the mean Chl *a* concentration in the box increased to its maximum of 0.47 mg·m$^{-3}$ (Fig. 7).

### 3.7 Mekong plume water

The MR is one of the largest rivers in the world. This river discharges into the SCS at about 10°N, 107°E with a mean annual discharge of 470 km$^3$ (Chen et al., 2010). From August 21 to 27, a strong eastward jet marked by high temperature (>29°C) and low salinity (<32) was recorded leaving the coast at about 11°N (Figs. 3(b)–3(h), Figs. 4(b)–4(h), and Figs. 7(d)–7(f)). More details can be found in Chen et al. (2010). Based on the daily discharge record at Kratie (in the lower reaches of the MR), August 3 marked the beginning of the 2007 flood season. The first peak discharge appeared on August 18 (Chen et al., 2010). Generally, it takes 2–4 weeks for MR water to reach the sampling point at 111.7°E, 14.2°N (Chen et al., 2010). The first Chl *a* peak appeared on August 22 (Fig. 2(c)), 19 days after the beginning of the 2007 flood season of the MR on August 3, and 4 days after the first peak discharge on August 18. This delay can explain the relationship between the eddy-like phytoplankton bloom and the MR plume.

## 4 Discussion

A cold eddy can fuel a cyclonic eddy-like phytoplankton bloom (Chen and Tang, 2012). It is still necessary to clearly describe eddy-like phytoplankton blooms to better understand the associated oceanic process. This study presents a clear record of a cyclonic eddy-like phytoplankton bloom. The bloom showed a complex composition roughly similar to the current of the eddy.

Previous investigations have not identified high surface Chl *a* in a cyclonic eddy-like shape on the outer southeastern shelf. Our results indicate that before the formation of the cold eddy, the surface phytoplankton bloom on the outer shelf was dramatically influenced by upwelling connected with the river plume (Figs. 2(d), 2(e) and Fig. 3(g)). Chen et al. (2010) showed that about 53% of the surface water in the western SCS originates from MR water diluted as it flows into the ocean. The transportation of the MR's freshened water into the western SCS takes more than 2 weeks (Chen et al., 2010). According to Chen's results, the horizontal advection of the nutrient-rich upwelled coastal waters and MR water fueled the eddy-like phytoplankton bloom. The cyclonic eddy's high-speed currents distributed the phytoplankton bloom to develop an eddy-like feature (Figs. 2(d)–2(h)). The

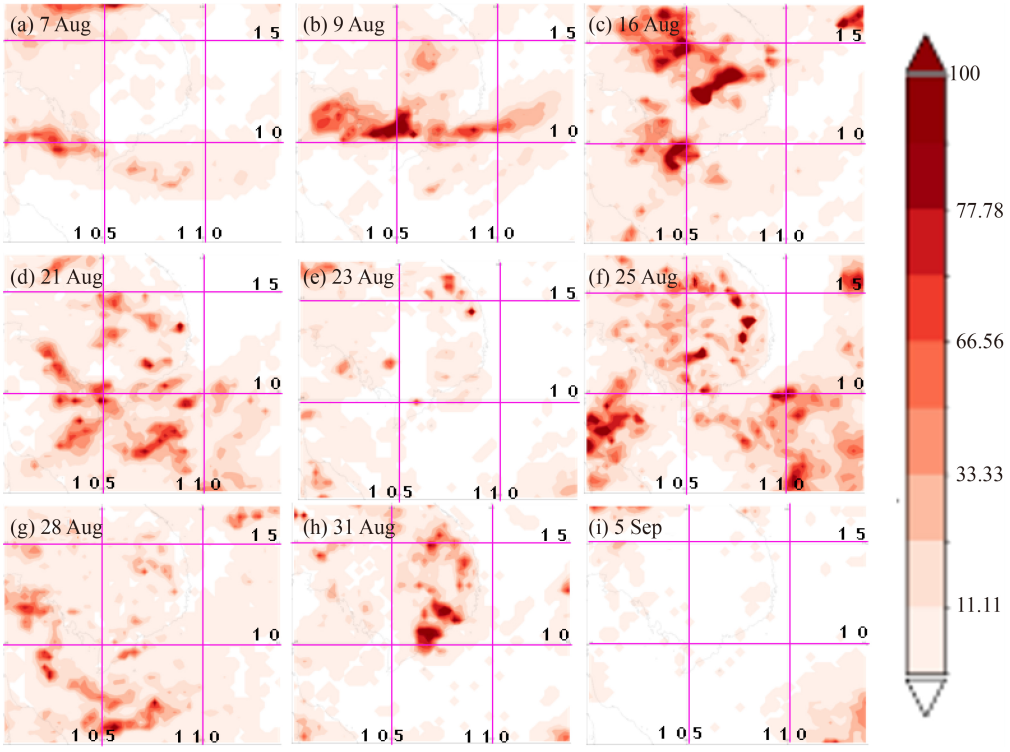


**Fig. 7** Rainfall rate. (a)–(c) Before the formation of the cyclonic eddy-like phytoplankton bloom; (d)–(e) form and mature of the eddy-like bloom; (f)–(i) decay of the bloom.

surface signature of the cyclonic eddy was not as evident as the signature below 25 m because of surface heating and the MR plume (Chen et al., 2010). The high Chl *a* in this area can only be explained by the north-eastward MR plume before the formation of the cyclonic eddy.

The south-west monsoon that occurs from June to September coincides with the wet season and the MR's maximum annual outflow (Grosse et al., 2010). During the south-west monsoon, nutrients are available due to coastal upwelling and the high runoff of the MR (Dippner and Loick-Wilde, 2011). The monsoon deflects the MR plume north-eastward toward the area where upwelling occurs (Bombar et al., 2010). Based on satellite chlorophyll data, Tang et al. 2004 assumed that the high Chl *a* patches around 12°N observed during the summer off the coast result from both MR runoff and upwelling of nutrient-rich waters (Tang et al., 2004a). The monsoon intensity is responsible for the geographical distribution of the water masses (Dippner et al., 2011). The cold filament does not simply persist throughout the entire summer but instead experiences 2–3 cycles of development and decay (Xie et al., 2007). Weakening of the south-west monsoon intensity from August 23 to 27 resulted in a weakening of the phytoplankton biomass and finally led to the decay and dispersal of the phytoplankton bloom. Our results show that the eddy-like surface phytoplankton bloom formed before the formation of the cyclonic eddy (Fig. 5, black arrow) and decayed before the eddy reached full maturity. This suggests that the surface distribution of phytoplankton may not be supported by the eddy pumped nutrients. We also checked the typhoon data during the bloom, and no typhoon occurred during this period; so, we have not considered the impact of a typhoon in this study.

The eddy edge has been identified as a critical channel for carbon sequestration in deep seas (Shih et al., 2015). High-speed eddy edge currents can transport high phytoplankton biomass several hundred kilometers into the open ocean (Mullerkarger et al., 1988). This process can form a long, high-chlorophyll biomass filament (Fig. 2). Such biomass-rich waters are probably important for the food chain dynamics of the outer south-eastern shelf and the coral islands or atolls in the oligotrophic SCS (Hu et al., 2003). There is a strong gradient in Chl *a* concentration between the biomass-rich filament and surrounding waters. As described by Belkin et al. (Belkin and O'Reilly, 2009; Belkin et al., 2009), this high Chl *a* filament is associated with a front. Further discussion on this topic is beyond the scope of this paper.

In previous studies, the eddy edge tended to reduce the signature of the biomass associated with the eddy. Without considering the effect of horizontal advection, the spatial difference of the biomass between the center and edge has generally been ignored (Chen and Tang, 2012; Wang et al., 2016). Diffusion from the nutricline provided nutrients for phytoplankton growth in the upper mixed layer, stimulating the growth of phytoplankton biomass in the surface layer of the center of the eddy.

Driven by the gradient of potential density between the eddy center and adjacent water and the effect of the rotation, high Chl *a* resulting from horizontal advection emerged at the edge of the eddy (Figs. 2(d)–2(f)). This resulted in a relatively low Chl *a* concentration at the eddy center but a relatively high concentration on the periphery of the eddy.

## 5 Conclusions

This study reveals a large eddy-like increase in Chl *a* in the western SCS. Before the formation of the cyclonic eddy, the eddy-like phytoplankton bloom was fueled mainly by strong offshore currents in the western SCS. After the formation of the cyclonic eddy, strong currents in the eddy distributed the phytoplankton bloom, exposing the circulation associated with the eddy. This eddy-like phytoplankton bloom was first detected on August 21 (Fig. 2(b)), then matured from August 22 to 24 (Figs. 2(c)–2(e)), and it decayed from August 28 to September 5 (Figs. 2(f)–2(h)), and disappeared after September 12. Our results suggest that this phenomenon is a potentially important conduit in carbon sequestration associated with the food chain dynamics of the outer south-eastern shelf and the coral islands or atolls in the oligotrophic SCS. Our research addresses the observational gap of an eddy-like phytoplankton bloom in the SCS. It also improves our understanding of eddy characteristics in the horizontal transfer of phytoplankton biomass and the distribution of nutrients from coastal water to the open ocean in the SCS.

**Acknowledgments** The present research was supported by the National Natural Science Foundation of China (Grant Nos. 31971480, 41406186, and 41406130), Key Special Project for Introduced Talents Team of Southern Marine Science and Engineering Guangdong Laboratory (Guangzhou) (Nos. GML2019ZD0303, and GML2019ZD0405) and Innovation Academy of South China Sea Ecology and Environmental Engineering, Chinese Academy of Sciences (Nos. ISEE2019ZR02 and ISEE2018ZD02). NASA's Ocean Color Working group provided the MODIS data. NASA Ocean Vector Winds Science Team provided the QuikScat wind-vector data. Analyses and visualizations used in this paper were produced with the Giovanni online data system, developed and maintained by the NASA GES DISC.

## References

Baith K, Lindsay R, Fu G, McClain C R (2001). Data Analysis System Developed for Ocean Color Satellite Sensors. Eos (Wash DC), 82(18): 202–204

Belkin I M, Cornillon P C, Sherman K (2009). Fronts in Large Marine Ecosystems. Prog Oceanogr, 81(1–4): 223–236

Bibby T S, Moore C M (2011). Silicate: nitrate ratios of upwelled waters control the phytoplankton community sustained by mesoscale eddies in sub-tropical North Atlantic and Pacific. Biogeosci Discuss, 7: 7505–7525

Bombar D, Dippner J W, Hai Nhu D, Lam Nguyen N, Liskow I, Loick-Wilde N, Voss M (2010). Sources of new nitrogen in the Vietnamese upwelling region of the South China Sea. J Geophys Res Oceans, 115: C06018

Chen G, Hou Y, Zhang Q, Chu X (2010). The eddy pair off eastern Vietnam: Interannual variability and impact on thermohaline structure. Cont Shelf Res, 30(7): 715–723

Chen X, Schallenberg C, Phillips H, Chase Z (2021). Biogeochemical characteristics of eddies in the East Australian Current depend on eddy type, history and location. J Mar Syst, 216(5): 103512

Chen Y, Tang D (2012). Eddy-feature phytoplankton bloom induced by a tropical cyclone in the South China Sea. Int J Remote Sens, 33(23): 7444–7457

Crawford W R, Brickley P J, Thomas A C (2007). Mesoscale eddies dominate surface phytoplankton in northern Gulf of Alaska. Prog Oceanogr, 75(2): 287–303

Dippner J W, Nguyen-Ngoc L, Doan-Nhu H, Subramaniam A (2011). A model for the prediction of harmful algae blooms in the Vietnamese upwelling area. Harmful Algae, 10: 606–611

Dippner J W, Loick-Wilde N (2011). A redefinition of water masses in the Vietnamese upwelling area. J Mar Syst, 84(1–2): 42–47

Everett J D, Baird M E, Oke P R, Suthers I M (2012). An avenue of eddies: quantifying the biophysical properties of mesoscale eddies in the Tasman Sea. Geophys Res Lett, 39: L16608

Grosse J, Bombar D, Doan H N, Nguyen L N, Voss M (2010). The Mekong River plume fuels nitrogen fixation and determines phytoplankton species distribution in the South China Sea during low- and high-discharge season. Limnol Oceanogr, 55(4): 1668–1680

Hu C M, Hackett K E, Callahan M K, Andrefouet S, Wheaton J L, Porter J W, Muller-Karger F E (2003). The 2002 ocean color anomaly in the Florida Bight: a cause of local coral reef decline? Geophys Res Lett, 30(3): 1151

Hu J, Gan J, Sun Z, Zhu J, Dai M (2011). Observed three-dimensional structure of a cold eddy in the southwestern South China Sea. J Geophys Res Oceans, 116: C05016

Kim D, Yang E J, Kim K H, Shin C W, Park J, Yoo S, Hyun J H (2012). Impact of an anticyclonic eddy on the summer nutrient and chlorophyll a distributions in the Ulleung Basin, East Sea (Japan Sea). ICES J Mar Sci, 69(1): 23–29

Klein P, Lapeyre G (2009). The oceanic vertical pump induced by mesoscale and submesoscale turbulence. Annu Rev Mar Sci, 1(1): 351–375

McGillicuddy D J Jr (2016). Mechanisms of Physical-Biological-Biogeochemical Interaction at the Oceanic Mesoscale. Annu Rev Mar Sci, 8(1): 125–159

McGillicuddy D J Jr, Johnson R, Siegel D A, Michaels A F, Bates N R, Knap A H (1999). Mesoscale variations of biogeochemical properties in the Sargasso Sea. J Geophys Res, 104(C6): 13381–13394

Mizobata K, Saitoh S I, Shiomoto A, Miyamura T, Shiga N, Imai K, Toratani M, Kajiwara Y, Sasaoka K (2002). Bering Sea cyclonic and anticyclonic eddies observed during summer 2000 and 2001. Prog Oceanogr, 55(1–2): 65–75

Mouriño-Carballido B (2009). Eddy-driven pulses of respiration in the

Sargasso Sea. Deep Sea Res Part I Oceanogr Res Pap, 56(8): 1242–1250

Muller-karger F E, McClain C R, Richardson P L (1988). The dispersal of the Amazons water. Nature, 333(6168): 56–59

Qiu D, Zhong Y, Chen Y, Tan Y, Song X, Huang L (2019). Short-term phytoplankton dynamicsduring typhoon season in and near the Pearl River Estuary, South China Sea. J Geophys Res Biogeosci, 124(2): 274–292

Shenoi S S C, Shankar D, Shetye S R (2004). Remote forcing annihilates barrier layer in southeastern Arabian Sea. Geophys Res Lett, 31(5): 1–4

Shih Y Y, Hung C C, Gong G C, Chung W C, Wang Y H, Lee I H, Chen K S, Ho C Y (2015). Enhanced particulate organic carbon export at eddy edges in the oligotrophic western North Pacific Ocean. PLoS One, 10(7): e0131538

Siegel D A, McGillicuddy D J Jr, Fields E A (1999). Mesoscale eddies, satellite altimetry, and new production in the Sargasso Sea. J Geophys Res, 104(C6): 13359–13379

Sun F L, Xia X M, Simon M, Wang Y S, Zhao H Y, Sun C C, Cheng H, Wang Y T, Hu S B, Fei J, Wu M L (2022). Anticyclonic eddy driving significant changes in prokaryotic and eukaryotic communities in the South China Sea. Front Mar Sci, 9: 773548

Tang D L, Kawamura H, Doan-Nhu H, Takahashi W (2004a). Remote sensing oceanography of a harmful algal bloom off the coast of southeastern Vietnam. J Geophys Res Oceans, 109: C03014

Tang D L, Kawamura H, Luis A J (2002). Short-term variability of phytoplankton blooms associated with a cold eddy in the northwestern Arabian Sea. Remote Sens Environ, 81(1): 82–89

Tang D L, Kawamura H, Van Dien T, Lee M (2004b). Offshore phytoplankton biomass increase and its oceanographic causes in the South China Sea. Mar Ecol Prog Ser, 268: 31–41

Wang G, Ling Z, Wang C (2009). Influence of tropical cyclones on seasonal ocean circulation in the South China Sea. J Geophys Res Oceans, 114: C10022

Wang L, Huang B, Chiang K P, Liu X, Chen B, Xie Y, Xu Y, Hu J, Dai M (2016). Physical-biological coupling in the western South China Sea: the response of phytoplankton community to a mesoscale cyclonic eddy. PLoS One, 11(4): e0153735

Wentz F J, Smith D K, Mears C A, Gentemann C L, Ieee I (2001) Advanced algorithms for QuikScat and SeaWinds/AMSR. In: Proceedings Igarss 2001: Scanning the Present and Resolving the Future, Vols 1–7: 1079–1081

Wu M L, Wang Y S, Wang Y T, Sun F L, Li X, Gu F F, Xiang J C (2022). Vertical patterns of chlorophyll a in the euphotic layer are related to mesoscale eddies in the South China Sea. Front Mar Sci, 9: 948665

Wu M L, Wang Y S, Wang Y Y, Sun F L, Li X M , Gu J D (2022b). A weak cold eddy influencing nitrogen form in the western part of the South China Sea. Regional Studies Mar Sci, 55: 102521

Xie S P, Chang C H, Xie Q, Wang D (2007). Intraseasonal variability in the summer South China Sea: Wind jet, cold filament, and recirculations. J Geophys Res Oceans, 112: C10008

Xie S P, Xie Q, Wang D X, Liu W T (2003). Summer upwelling in the South China Sea and its role in regional climate variations. J Geophys Res Oceans, 108(C8): 3261